Improved Artificial Rabbits Algorithm for Positioning Optimization and Energy Control in RIS Multiuser Wireless Communication Systems

Ahmed S. Alwakeel, Mohamed I. Ismail, Mostafa M. Fouda, *Senior Member, IEEE*, Abdullah M. Shaheen, and Adel Khaled

Abstract—An innovative method to raise wireless communication systems' efficiency is to use Reconfigurable Intelligent Surface (RIS). Unfortunately, determining the quantity and locations of the RIS elements continues to be difficult, requiring a clever optimization framework. Concerning the practical overlap between the related multi-RISs in wireless communication systems, this paper attempts to minimize the number of RISs while considering the average possible data rate and technological constraints. In this regard, a novel Enhanced Artificial Rabbits Algorithm (EARA) is developed to minimize the number of RISs to be installed. The novel EARA is inspired by the natural survival strategies of rabbits, including detour eating and random concealment. A more effective method of exploring the search space around the best solution so far is produced by the suggested EARA by combining an upgraded Collaborative Searching Operator (CSO) arrangement. Also, an adaptive time function is included to increase the effect of this exploitation tactic by the increasing number of iterations. The simulation results show that the suggested EARA is highly efficient in reaching the maximum success rate of producing the smallest number of RISs under various feasible rate threshold settings. When EARA is compared to standard Artificial Rabbits Optimizer (ARO), Growth Optimizer (GO), Artificial Ecosystem Optimizer (AEO), and Particle Swarm Optimization (PSO), the average number of RISs is improved by 5.32%, 6.7%, 16.73%, and 20.06%, respectively. Furthermore, according to simulation data, the EARA outperforms AEO, GO, ARO, and PSO in terms of success rate at  $\delta = 1.4$  by 6.66%, 6.66%, 45.43%, and 99%, respectively.

Reconfigurable intelligent surfaces, Wireless communication, Artificial Rabbits Algorithm, Achievable rate limitation.

#### I. Introduction

While the 5th-generation cellular network (5G) continues to be deployed globally, academic and industry communities

The work of Mostafa M. Fouda was supported by the National Science Foundation of the USA under Award No. 2210252. (Corresponding author: Mostafa M. Fouda.)

Ahmed S. Alwakeel, Abdullah M. Shaheen, and Adel Khaled with the Department of Electrical Engineering, Faculty Engineering, University, P.O. Box: of Suez 43221. Suez. (emails: ahmed.alwakeel@eng.suezuni.edu.eg, abdullah.mohamed.eng19@suezuni.edu.eg, and adel.khaled@eng.suezuni.edu.eg). Mohamed I. Ismail is with the Department of Electronic Engineering & Communication Technology, Modern Academy for Engineering, Egypt (e-mail: mohamed.ismail@eng.modern-academy.edu.eg).

Mostafa M. Fouda is with the Department of Electrical and Computer Engineering, College of Science and Engineering, Idaho State University, Pocatello, ID 83209, USA (e-mail: mfouda@ieee.org).

Copyright ©2024 IEEE. Personal use of this material is permitted. However, permission to use this material for any other purposes must be obtained from the IEEE by sending a request to pubs-permissions@ieee.org.

have focused on imagining the post-5G future, also known as Beyond 5G (B5G). The upcoming sixth-generation cellular networks (6G) is now in the spotlight, as it is intended to meet even more demanding requirements than its predecessor [1]–[5]. These requirements include incredibly high data speeds, energy efficiency, flawless global coverage and connectivity, outstanding dependability, and low latency. But meeting these demanding standards with current technological trends—like Enhanced Mobile Broadband (eMBB), Ultra Reliable Low Latency Communications (URLLC), and massive Machine Type Communications (mMTC)—tailored for 5G services poses difficulties begging for innovative solutions [4], [6]–[8]. Using the RIS in wireless communications is one of these creative solutions [9], [10].

With arrays of antenna elements, RISs can assist in establishing a Line-of-Sight (LOS) link between the transmitter and the receiver even in the presence of obstacles or when the received power from the direct path is insufficient to create a dependable connection [10]–[13]. Hybridization holds great promise with its potential to accomplish significant network capacity growth cost-effectively and guarantee sustainability going forward. However, even with its great potential, new challenges arise when RIS is integrated into wireless networks, which must be successfully overcome. They consist of precise channel estimation, reflection mechanism optimization, and the challenging work of installing RIS while maintaining the integrity of communication design principles [4]. The effectiveness and efficiency of RISs are significantly impacted by their placement. The number of access points may be decreased by optimally locating the RISs. As such, one of the issues facing the deployment of RISs [14] is the selection of these places. We summarize the related work, then go into a motivation and research problem, and end the introduction section with a quick discussion of the research gap and the paper's main contribution.

## A. Related Work

Numerous studies have been conducted on the use of optimization algorithms for RIS placement. With the aid of RISs, the authors in [15] examined how well range estimation performs for a cellular user in a millimeter-wave (mm-wave) network utilizing received signal strength indicator (RSSI) measurements. First, they present the best practice for RIS deployment, which is to minimize the total likelihood of

1

blocking both the user's connection to the base station (BS) and the RIS connection. The authors then go on to describe a method of range estimation based on specific constraints. In [16], the authors discussed localization algorithms based on near-field (NF) and offered RIS as a solution to a particular issue. Accurate and simultaneous localization of several energy-constrained devices is a crucial need in a variety of location-based Internet of Things (IoT) applications.

One paper that suggests and tackles the optimization problem for RIS-aided networks is [17] in which the authors created a new optimal location-based RIS selection criteria for RIS-aided wireless networks. They boost the signal-to-noise ratio (SNR) for a power path loss model for outdoor communications and an exponential path loss model for indoor communications. n [18], an alternative optimization problem was also put forth. The authors utilized the LoS link between nearby RISs to construct a multi-hop cascaded LoS link between the BS and the user. A fairly recent study on RIS-aided network performance optimization is reported in [19]. By dynamically controlling the on-off status of each RIS and modifying the RIS's reflection coefficient matrix, the network's energy efficiency was maximized. Also, multiple RISs are deployed to handle wireless users.

Further details on optimization problems in RIS-aided networks with multiple RISs may be found in [20] and [21]. A multi-RIS-assisted system for indoor and outdoor communications was examined by [22]. To achieve the lowest complexity of transmission, the authors proposed a RIS selection technique that selects the RIS with the maximum SNR to support the communication. However, optimizing the RIS phase shifts is a major challenge in real-world RIS-assisted systems [23]-[29]. Recently, the RIS setup of point-to-point multiple-input multiple-output (MIMO) systems has been enhanced in [23] to boost the channel capacity. A URLLC system with a dedicated RIS assisting the BS in transmitting brief packets in a Finite Blocklength (FBL) scenario was explored in [30]. A greedy algorithm was used in [31] to solve the user grouping problem, and a semi-definite relaxation technique was used to address the proposed optimization problems. Authors in [32] examined a RIS-assisted multiple-input single-output (MISO) system to adjust the BS transmit beamforming and the passive beamforming at the RIS to optimize the total achievable rate in the infinite blocklength regime. Joint relay selection and RIS reflection coefficient optimization were studied in cooperative networks [33].

In [34], the authors presented a novel method for organizing elements in centralized RIS, a set of groups comprised of nearby RIS elements with the same reflection coefficient. They proposed an efficient transmission protocol based on this grouping technique, wherein the aggregate channel estimation for each group is the only thing needed. The overhead of training is greatly decreased by using this method. In [35], the authors use a single RIS to optimize both the transmit beamforming vectors at the BS and the reflection coefficient vector at the RIS to reduce the total transmit power. To get a locally optimal solution in this context, an effective approach based on the alternating direction method of multipliers (ADMM) and second-order cone programming (SOCP) is presented. Authors

of [36] described how an RIS-assisted downlink multi-user system's power distribution and phase shifts were designed in tandem to optimize energy efficiency.

For multi-hop RIS-assisted communication systems, the authors of [37] suggested a hybrid beamforming approach to increase the coverage range in the terahertz frequency spectrum. The authors of [38] examined the effect of phase noise on the optimization problem of RIS-assisted communication systems across generalized fading channels. Furthermore, it has been demonstrated by the authors of [39] that uniformly dispersed deployments of the same magnitude outperform centralized RIS deployments in terms of performance. Furthermore, [40] examined single-RIS and multi-RIS deployment approaches for RIS-assisted relay systems and showed that a higher system capacity could be attained by multi-RIS deployment.

Nevertheless, the research in [41] demonstrated that the centralized deployment outperforms the dispersed one in terms of capacity description. These investigations compared centralized (single-RIS) versus scattered (multiple-RIS) installations rather than site optimization. The study in [42] indicates that the closer the RIS is to the user or BS, the higher the SNR that may be yielded; however, the impact of RIS orientation is ignored because the RIS unit was considered an isotropic radiator.

The authors of [43] optimize the positioning of RISs to maximize the coverage area in an indoor environment. They offer 3D hybrid beamforming at the BS and phase adjustment at the RISs. These tasks are simultaneously carried out at the RISs and the BS using low-complexity codebook-based 3D beam scanning. The transmit precoder and the placement of active and passive components in the hybrid reconfigurable intelligent surfaces' coefficients are cooperatively designed by the authors of [44] in order to maximize the SNR. The study conducted by the authors of [45] focuses on a RISassisted downlink communication system that can transmit and reflect simultaneously. The system seeks to maximize the sum rate of users in NLOS areas by optimizing the beamforming at the BS and the RISs. When there is just one RIS per sector, the authors of [46] demonstrate that the best location for RIS to attain broader coverage is precisely opposite to the BS. They deduce the possible sum rate in the presence of optimal, discrete, and random phase shifters at RIS by suggesting a novel beamforming architecture for RIS-assisted cellular systems. A maximization problem was developed by the authors in [47] to aid in the optimization of RIS placement and discrete phase design, which are bounded by the coverage probability.

Recently, Wang *et al.* presented the novel Artificial Rabbits Algorithm (ARA), which draws inspiration from rabbits' innate coping mechanisms as detour feeding and spur-of-themoment hiding. This ARA's main motivator highlights the features that render it effective in solving numerous optimizing issues [48]. The rabbit is forced to eat grass that grows next to the nests as part of the detour foraging strategy to keep predators from finding their home. Furthermore, a rabbit may use the stochastic concealing technique to select any of its private residences at random to flee to, which might lessen the likelihood that potential adversaries would catch

it. Rabbits' energy levels might also wane, causing them change their planned foraging behavior in favor of carel hiding [49], [50]. To reduce the number of RIS that m be deployed, a unique EARA is created in this study. I survival tactics used by rabbits in nature, such as det feeding and haphazard hiding, served as inspiration for proposed EARA. It combines an improved CSO arrangem with an adaptive time function to generate a more effect way of exploring the search space around the best solution far. The main contribution of the paper is shown below.

### B. Motivation of the Research Problem

The IoT involves the interconnection of a multitude devices and sensors, which are often deployed in dive environments with varying signal strengths, interference, and propagation conditions. RIS introduces a new paradigm in wireless communication that can enhance the connectivity and communication quality of IoT devices. RIS can optimize communication paths and mitigate issues like signal attenuation, interference, and multipath fading. Additionally, RIS optimization improves energy efficiency by optimizing communication paths and reducing the need for IoT devices to transmit signals over longer distances.

Therefore, the optimization of RIS placement has become an essential undertaking as RIS deployment picks up steam. In order to take advantage of their reflected qualities and improve the wireless environment, RIS elements must be strategically positioned. Finding the best places to install RIS parts in a certain environment is the basic idea behind RIS placement optimization. The objective is to intelligently reflect and refract electromagnetic waves in order to alter signal propagation and establish the desired communication characteristics.

### C. Research Gap and Main Contribution

Previous studies have only used the RIS to extend coverage, considering its position; however, there is limited research done on how to deploy the RIS to further spread out cell coverage. Additionally, without regard to the RIS area, the majority of research efforts in the literature concentrate on solving conventional wireless communication issues under the new premise of an assisted metasurface solution. Last but not least, there has not been adequate investigation of how to implement RIS optimally in a scenario with several users. Considering the aforementioned, to fill this gap, this paper explores the RIS deployment position optimization for wireless communication systems assisted by multiple RISs and serving multi-users. We characterize a facility placement challenge as a RIS deployment problem, which enables us to figure out where to deploy RIS and optimize the wireless network's total data flow. We also study how various parameters affect communications facilitated by RIS. Furthermore, a novel robust algorithm for jointly determining the phase shift coefficients, number, and locations of RISs is proposed in order to reduce the total number of RISs exposed to the average possible data rate. The efficiency of the proposed technique is verified through comparison with baselines in a multiRIS-aided wireless communication system.



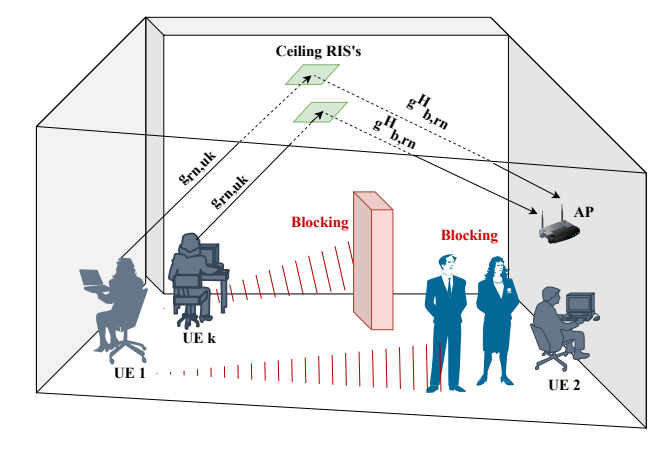


Fig. 1: System model.

The main contributions made in this work are as follows:

- Advanced optimization framework: Introduces an advanced model considering wireless communication systems employing RIS assistance to provide reflecting pathways that improve received power at multi-user equipment.
- Real-world application: Achieve the highest possible rate with the minimum RISs considering real-world system restrictions by ascertaining the number, positions, and phase shift coefficient of RISs.
- 3) Novel EARA optimizer: Develop a novel efficient EARA utilizing upgraded CSO arrangements and adaptive time functions to enhance exploration of the solution space, improving the algorithm's effectiveness in reaching optimal solutions.
- 4) Superior Performance: Demonstrates EARA's superiority over contemporary optimization algorithms (AEO [51], GO [52], ARO, PSO) through comprehensive simulations, showcasing its ability to minimize the number of RISs required for optimal system performance.

The rest of the paper is organized as follows. The system model is described in Section II. The proposed EARA algorithm for optimal placement of RIS elements is presented in Section III. Numerical results are provided in Section IV to verify the performance of the proposed algorithm, whereas conclusions are presented in Section V.

Notation: We use boldface (lower case) for column vectors,  $\boldsymbol{x}$ , (upper case) for matrices,  $\boldsymbol{X}$ . Let  $\boldsymbol{X}^{-1}$ ,  $\boldsymbol{X}^{\mathrm{H}}$ ,  $\boldsymbol{X}^{\mathrm{T}}$ , and  $\boldsymbol{X}^{\dagger}$  denote the inverse, conjugate transpose (Hermitian), transpose, and pseudo-inverse of  $\boldsymbol{X}$ , respectively. The matrix trace function is denoted by  $\operatorname{tr}(\boldsymbol{X})$ .  $\|.\|$  is the Euclidean norm. A circularly symmetric complex Gaussian random vector  $\boldsymbol{x}$  is denoted by  $\boldsymbol{x} \sim \mathcal{CN}(\mu, \gamma)$ , where  $\mu$  is the mean and  $\gamma$  is the covariance matrix. The set of all complex numbers is denoted by  $\mathbb{C}$ . with  $\mathbb{C}^{N\times 1}$  and  $\mathbb{C}^{N\times M}$  being the generalizations to vectors and matrices, respectively. The  $M\times M$  identity matrix is written as  $\boldsymbol{I}_M$ .

## II. SYSTEM MODEL

We propose a multi-RIS-aided wireless communication system in indoor settings such as stadiums and halls, as seen in

Figure 1. In this system, K single-antenna user equipment (UE) connects with a single-antenna Access Point (AP) in orthogonal time slots with the help of N equal-size RISs. Our supposition is that each RIS installed on the ceiling is a homogeneous planar array with M reflecting elements.

#### A. Communication Channel Model

Let  $\boldsymbol{\xi}_n=(\xi_{n,1},\xi_{n,2},...,\xi_{n,M})^T$  is referred to the phase shift coefficient of RIS n, and  $\boldsymbol{\Xi}_n=diag\{e^{j\xi_{n,1}},e^{j\xi_{n,2}},...,e^{j\xi_{n,M}}\}$  is used to represent the phase shift coefficient matrix of RIS n. Along with that, we also designate  $\boldsymbol{g}_{b,r_n}\in\mathbb{C}^{M\times 1}$  as the channel vector from RIS n to the AP,  $\boldsymbol{g}_{r_n,u_k}\in\mathbb{C}^{M\times 1}$  as the channel vector from UE k to RIS n, and  $g_{b,u_k}\in\mathbb{C}^{1\times 1}$  as the channel from UE k to the AP. Both UE-RIS and RIS-AP lines employ the Rician fading channel model. Consequently,  $\boldsymbol{g}_{b,r_n}$  is written as

$$oldsymbol{g}_{b,r_n} = S_{b,r_n} \left( \sqrt{\frac{\epsilon}{\epsilon+1}} oldsymbol{e}_n(\gamma_n, \phi_n) + \sqrt{\frac{1}{\epsilon+1}} oldsymbol{f}_{b,r_n} \right) \quad (1)$$

where  $S_{b,r_n}$  stands for the path loss between RIS n and the AP, the Rician factor is represented by  $\epsilon$ . The array response of RIS n is denoted by  $e_n \in \mathbb{C}^{M \times 1}$ ; where  $\gamma_n$  is the azimuth angle and  $\phi_n$  is the elevation angle of departure for the link between RIS n and the AP.  $f_{b,r_n}$  represents the direct components and their elements are chosen from  $\mathfrak{CN}(0,1)$ . Similarly,  $g_{r_n,u_k}$  is expressed as

$$g_{r_n,u_k} = S_{r_n,u_k} \left( \sqrt{\frac{\epsilon}{\epsilon+1}} e_n(\gamma'_n, \phi'_n) + \sqrt{\frac{1}{\epsilon+1}} f_{r_n,u_k} \right)$$
(2)

where  $\gamma_n'$  and  $\phi_n'$  is the azimuth and elevation angle, respectively, for the link between RIS n and UE k. The direct channel between user k and the AP is stated as

$$g_{b,u_k} = S_{b,u_k} f_{b,u_k} (3)$$

where the path loss between UE k and the AP is indicated by  $S_{b,u_k}$ . The received signal at the AP from RIS n is given by

$$z_{AP,n} = (\mathbf{g}_{b,r_n}^H \mathbf{\Xi}_n \mathbf{h}_{r_n,u_k} + g_{b,u_k}) x + v \tag{4}$$

where x is the transmitted symbol with power  $p_k$ ,  $\mathbf{g}_{b,r_n}^H \mathbf{\Xi}_n \mathbf{h}_{r_n,u_k}$  is the effective channel including RIS n phase shift and  $g_{b,u_k}$  is the channel gain of the direct path, v represents the noise with  $\mathcal{NC}(0,\sigma^2)$ . The received SNR is given by

$$SNR = \left(\frac{p_k |\alpha_{b,u_k} g_{b,u_k} + \sum_{n=1}^{N} \alpha_{b,r_n} \boldsymbol{g}_{b,r_n}^H \boldsymbol{\Xi}_n \boldsymbol{g}_{r_n,u_k}|^2}{\sigma^2}\right)$$

The achievable sum rate of user k is shown in (6). Where the parameters  $\alpha_{a,n}$  and  $\alpha_{a,k}$  satisfy

$$\alpha_{b,r_n} = \begin{cases} 0 & \text{if the link between RIS } n \text{ and} \\ & \text{AP is blocked} \\ 1 & \text{otherwise} \end{cases}$$
 (7)

$$\alpha_{b,u_k} = \begin{cases} 0 & \text{if the link between RIS } n \text{ and} \\ & \text{AP is blocked} \\ 1 & \text{otherwise} \end{cases}$$
 (8)

### B. Problem Formulation

In this paper, we introduce a method for concurrently optimizing the quantity, distribution, and RIS reflection patterns in an RIS-aided wireless communication system. The resulting parameters are evaluated to demonstrate the effectiveness of the proposed approach. The suggested method reduces the quantity of RIS subject to the feasible rate under certain system restrictions, which is represented as

$$\begin{array}{ll}
minimize & N \\
N, \{u_1, z_n\} \in \mathcal{E}
\end{array} \tag{9}$$

subject to

$$\frac{1}{K} \sum_{k=1}^{K} R_k \ge \delta \tag{10a}$$

$$x_{min} \le x_n \le x_{max}, \forall n \in \{1:N\}$$
 (10b)

$$y_{min} \le y_n \le y_{max}, \forall n \in \{1:N\}$$
 (10c)

$$min\{|x_n - x_c|, |y_n - y_c|\} \ge L, \forall n, c \in \{1:N\}$$
 (10d)

$$N_{min} \le N \le N_{max} \tag{10e}$$

where  $\{x_n, y_n\}$  is the location of RIS n and L denote the size length of each RIS. The constrain (10a) ensures that the achievable rate for all users is larger than  $\delta$ , (10b) and (10c) illustrate the location restrictions of the RISs. We use (10d) to ensure that RISs are not overlapping, and (10e) ensures that the number of RISs is between  $[N_{min}, N_{max}]$ .

# III. PROPOSED EARA FOR OPTIMAL PLACEMENT OF RIS ELEMENTS

ARO algorithm provides a straightforward implementation and exhibits rapid convergence towards favorable solutions by identifying the top participants within the search region. The ARO's performance is effectively validated across a variety of scenarios, including 23 benchmark functions and 5 engineering design problems [48]. These tests showcase the algorithm's proficiency in solving global optimization problems. The ARO algorithm stands out for its simplicity in implementation and the straightforward nature of its mathematical models. These characteristics render it well-suited for addressing challenges posed by nonlinear, high-dimensional, and multimodal problems commonly encountered in literature. Examples of these successful applications include improving the smart IoT environment against botnet attacks [53], optimal power flow in electrical power systems [54], optimal Designing of hybrid microgrid [55], parameter calibration of flood routing [56], dispatch in combined heat and power systems [57], load frequency control in isolated microgrids [58], medical data classification and emergency monitoring in hospitals [59], Sizing of Water Storage Tank integrated with Photovoltaic Pumping System [60]. In this section, the proposed EARA algorithm is presented in the first part, while its adoption for handling the proposed model is illustrated in the second part.

$$R_k = \mathbf{E} \left\{ \log_2 \left( 1 + \frac{p_k |\alpha_{b,u_k} g_{b,u_k} + \sum_{n=1}^N \alpha_{b,r_n} \mathbf{g}_{b,r_n}^H \mathbf{\Xi}_n \mathbf{g}_{r_n,u_k}|^2}{\sigma^2} \right) \right\}$$
 (6)

## A. Proposed EARA

Detour feeding and random hiding are two tactics that the ARA mimics from how rabbits behave in their natural environment. The diversion foraging strategy is initially mimicked, where the rabbit is forced to eat the grass around neighbouring nests, giving the capability to quickly hide from attackers. Secondly, by employing the randomized concealment technique, it may be possible to lessen the likelihood that an enemy might catch a rabbit. Thirdly, when energy is depleted, rabbits may be forced to switch from their detour eating strategy to an irregular hiding technique [48]. Each iteration modifies the population of rabbits' positions in accordance with the fitness function. The search solutions indicate the locations of the rabbits, which are modified and upgraded as the process goes on. According to equation (11), each place in the initial population is assigned a randomly chosen site inside the search space:

$$AR_k = Lo + R_1 \times [Up - Lo], \quad k = 1: N_{AR}$$
 (11)

where  $AR_k$  indicates the place of every artificial rabbit indexed by (k). Lo and Up are the lower and upper limits regarding the control variables.  $N_{AR}$  refers to the population size regarding the number of the considered artificial rabbits.  $R_1$  is a vector of Dim dimensions which includes random continuous values between 0 and 1.

According to the ARA's detour foraging strategy, every pursuing rabbit decides to trade places with a different one that is randomly selected from the swarm and combines distraction. The forage that rabbits use as a diversion is described as shown in equations (12), (13), (14).

$$v(m) = \begin{cases} 1, & \text{if } m = g(\psi), \\ 0, & \text{otherwise.} \end{cases},$$

$$m = 1 : Dim \& \psi = 1 : [z_3, Dim]$$
(13)

$$q = Randp(Dim) \tag{14}$$

where the current iteration is denoted by t; The k-th rabbit's new and old positions are designated as  $AR_k^*$  and  $AR_k$ , respectively;  $ST_N$  defines the standard function associated with the normal distribution;  $z_1$ ,  $z_2$  and  $z_3$  comprise three randomly selected values spanning the interval [0, 1], and  $t_{max}$  provides the greatest number of repetitions. Randp is a randomizing permutation function.

A rabbit usually digs many tunnels close to the nest to use as cover when fending off predators. This is illustrated by the formula shown in equations (15), (16).

$$Bu_{k,m}(t) = AR_k(t) \times (1 + (z_4 \times \frac{1 + t_{max} - t}{t_{max}})\mu),$$

$$k = 1 : N_{AR} \& m = 1 : Dim$$
(15)

$$\mu(m) = \begin{cases} 1, & \text{if } m = k, \\ 0, & \text{otherwise.} \end{cases}, \quad m = 1 : Dim$$
 (16)

where  $z_4$  appears to be an integer chosen at random from [0, 1];  $Bu_{k,m}$  is the m-th burrow of the k-th rabbit. Based on this characteristic, these burrows are originally constructed in a rabbit's larger surroundings. This region gets smaller as the number of iterations increases.

Rabbits need to locate a secure area to dwell in order to continue. They are so discouraged from picking a hole at random from those present that they must bury themselves in it. The algebraic equation shown below can be used to illustrate this randomized hiding method:

$$AR_k^*(t+1) = AR_k(t) + v \times \left(e - e^{\left(\frac{t-1}{t_{max}}\right)^2}\right) \times sin(2\pi z_2)(z_5 \times Bu_{k,m}(t) - AR_k(t)), k = 1: N_{AR}$$
(17)

If diversion foraging or arbitrarily hiding are successful, the kth rabbit's position is changed as shown in equation (18) in next page.

Moving from the discovery phase related to detour foraging to the exploit stage related to randomized concealment includes an energy component. The following definition applies to the energy factor (EF):

$$EF(t) = 4 \times \left(\frac{t_{max} - t}{t_{max}}\right) \times ln\frac{1}{Zr}$$
 (19)

In order to enhance the searching skills while avoiding local optima, a CSO arrangement is adopted in order to effectively support the exploration of the best solution so far. In order to incorporate it, equation (12) is modified by substituting the current searching rabbit  $(AR_k(t))$  with the best solution so far  $(AR_S)$  as shown in equation (20). In the suggested EARA model, both equations are activated, and an adaptive time function is modeled in equation (21).

$$TF(t) = \frac{t}{2 \times t_{max}} \tag{21}$$

where TF is the suggested time function in terms of the current iteration. Based on its updated value, there is a transfer between the standard detour foraging form in equation (12) and the proposed model incorporating the CSO in equation (20). With the increasing number of iterations, the probability of activating the proposed CSO model is gradually increasing, as is the effect of the exploitation tactic. Figure 2 displays the main steps of the proposed EARA for solving the optimal placement of RIS elements.

## B. Adoption of the Proposed EARA for Optimal Placement of RIS Elements

In the proposed optimization framework, equation (9) represents the objective function, which is the minimization of the

$$AR_k^*(t+1) = AR_m(t) + (AR_k(t) - AR_m(t)) \times v \times (e - e^{(\frac{t-1}{t_{max}})^2}) \times sin(2\pi z_2) + ST_N \times round(\frac{1}{2} \times (\frac{5}{100} + z_1)),$$

$$m, k = 1 : N_{AR}, \ m \neq k$$
(12)

$$AR_k(t+1) = \begin{cases} AR_k(t), & \text{if } f(AR_k(t) \le f(AR_k^*(t+1), \\ AR_k^*(t+1), & f(AR_k(t) > f(AR_k^*(t+1)) \end{cases}$$
(18)

$$AR_{k}^{*}(t+1) = AR_{m}(t) + (AR_{S} - AR_{m}(t)) \times v \times (e - e^{(\frac{t-1}{t_{max}})^{2}}) \times sin(2\pi z_{2}) + ST_{N} \times round(\frac{1}{2} \times (\frac{5}{100} + z_{1})),$$

$$m.k = 1: N_{AR}, \quad m \neq k$$
 (20)

quantity of RISs, where the design variables are N, x, and y. Based on that, there are limitations on these variables as displayed in Equations (10e), (10b), and (10c), respectively. On the other side, inequality constraints due to independent variables are handled where the constraint (10a) ensures that the achievable rate for all users is larger than and Equation (10d) to ensure that RISs are not overlapping. In order to adopt the proposed EARA for solving the proposed model, different enhancements should be implemented, as displayed in Block A in Figure 2 as follows:

First, each solution vector, the rabbit position, is assigned to the design variables, which are the number of RIS to be placed and their distribution patterns in the model of the RIS-aided wireless communication system that is being shown. These control variables come in two varieties, where the installed locations are continuous and the number of RIS is an integer. The number of RIS is treated as a continuous range since the EARA typically operates in a continuous framework before being rounded to the next integer.

Second, the fitness function measures how well a solution performs when compared to the optimization aim. Also, the violating control variable is replaced in this study with a randomly chosen value that falls within the realistic bounds of the control variable. As a result, the limitations shown in equations (10b) to (10d) are assured.

Third, penalty components are being added to the function of fitness to account for the dependent variable limitations provided in equations (10a) and (10e). As a result, Equation (9) is extended to express the fitness function (f) as follows:

$$f = N + Py_1 \Delta GH + \sum_{n=1}^{N} \sum_{c=1}^{N} Py_2 \Delta GK_{n,c}$$
 (22)

where  $Py_1$  and  $Py_2$  are penalty factors,  $\Delta GH$  and  $\Delta GK$  are defined as follows:

$$GH = \begin{cases} 0, & \text{if } \frac{1}{K} \sum_{k=1}^{K} R_k \ge Q, \\ |Q - \frac{1}{K} \sum_{k=1}^{K} R_k|, & otherwise \end{cases}$$
(23)

According to the aforementioned framework, unrealistic solutions that are unable to satisfy one or more restrictions are going to receive a high fitness score, which makes it unlikely that they will be carried over to the subsequent iteration.

The complete pseudo-code of the proposed methodology is attached in the appendix section VI.

### IV. NUMERICAL RESULTS

In this section, we perform numerous case studies to evaluate the superiority of the EARA algorithm over the other techniques. These methods were all developed with the goal of simultaneously optimizing RIS quantity and location. Take into consideration a wireless communication system with several RISs in which users are dispersed randomly within a square with vertices of [0, 0, 0], [0, 10, 0], [10, 10, 0], and [10, 10, 0] m. The RISs are arranged within the square with vertices of [0, 0, 10], [0, 10, 10], [10, 0, 10], and [10, 10, 10] m. Four vertices at [0, 0, 0], [0, 0, 2.25], [10, 0, 2.25], and [10, 0, 0] m specified the location of the wall, and the coordinates of the AP were also set to [5, -10, 1] m (c.f. Figure 1).

Path loss modeling is done as follows:  $PL = PL_0 - 10\beta\log(\frac{d}{d_0})$ ; path loss at reference distance  $d_0 = 1m$  is  $PL_0 = 20dB$ ; d is the distance between transmitter and receiver; and the path loss exponents of the UE-RIS-AP link and the UE-AP link are set to  $\beta = 2.2$  and  $\beta = 4$ , respectively. Each RIS in the simulation has M = 100 elements, and there are K = 20 single antenna users. The transmit power of user k is  $p_k = 1mW$ , the size length of each RIS element is L = 0.3m, and the Rician factor is  $\epsilon = 10$ .  $\sigma^2$  is the noise power for SNR = -23dB and number of RISs is between  $N_{min} = 1$  and  $N_{max} = 10$ .

There are four subsections within the simulation section. The box plot in the first part displays the number of RIS elements that are retrieved by various algorithms, with the lowest, median, and maximum values displayed. In the second part, the number of RISs for different optimization algorithms is displayed. The convergence plot presented in the third section illustrates the fitness value. In the end, each optimization technique's success rates are presented.

The box plot <sup>1</sup> of the number of RISs for various optimization strategies is shown in Figure 3, which compares the

<sup>&</sup>lt;sup>1</sup>A box plot presents the data set's five-number summary. These numbers are minimum, first quartile, median, third quartile, and maximum. The first quartile to the third quartile is where we draw a box in a box plot. Through the box at the median is a vertical line.

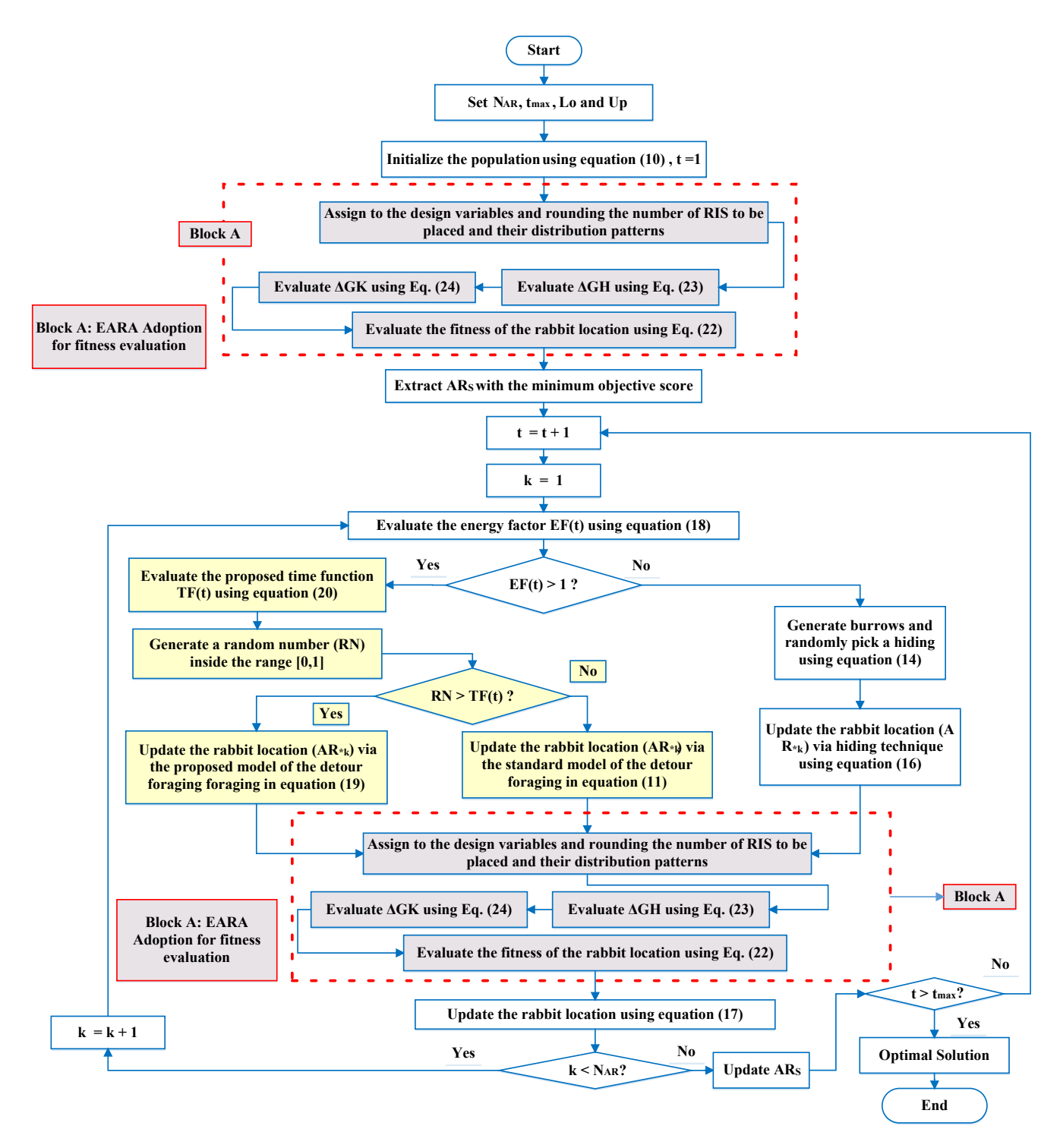


Fig. 2: Main steps of the proposed EARA.

$$GK_{n,c} = \begin{cases} 0, & \text{if } \min\{|x_n - x_c|, |z_n - z_c|\} \ge L, \\ |L - \min\{|x_n - x_c|, |z_n - z_c|\}|, & \text{otherwise} \end{cases}$$
 (24)

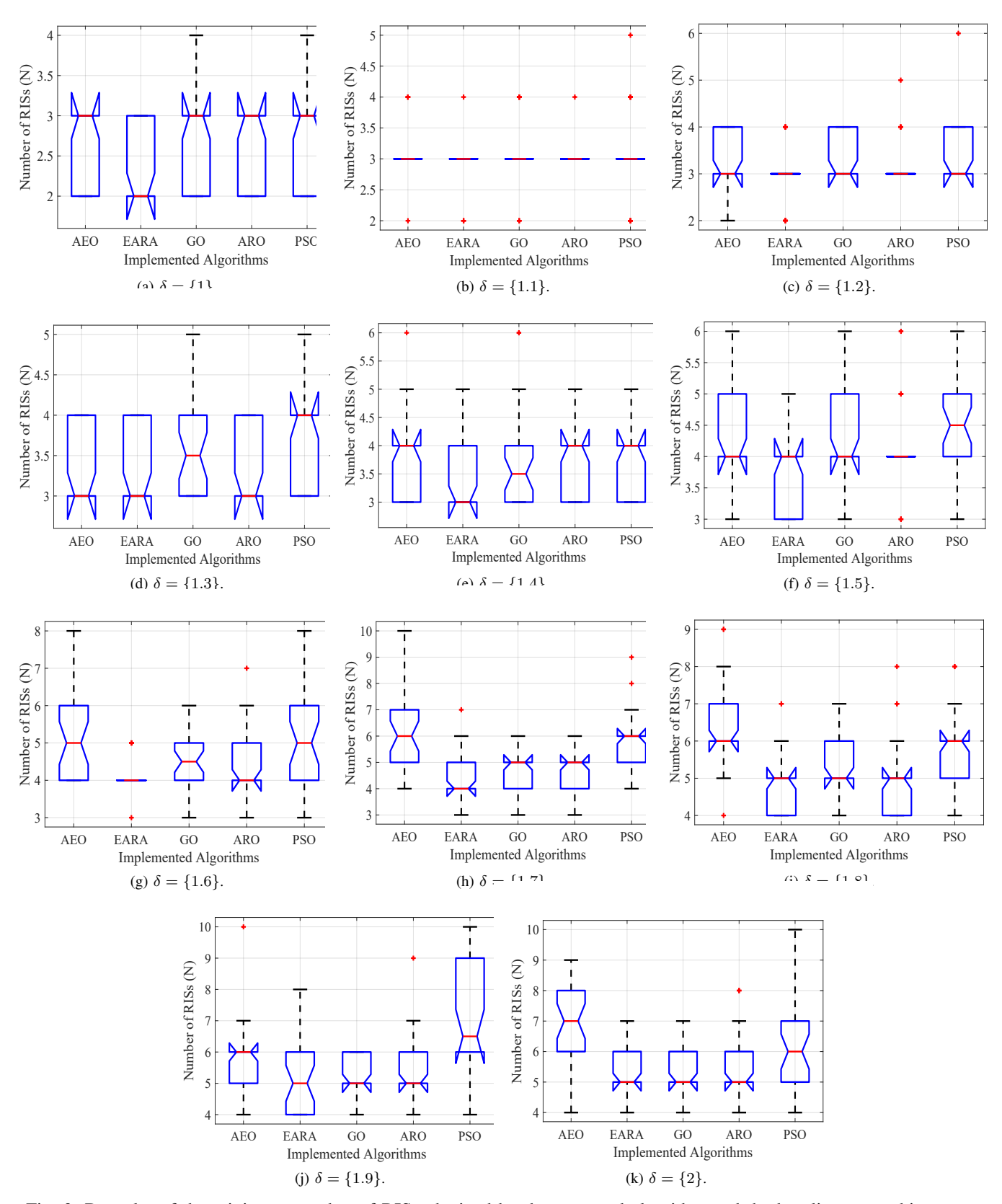


Fig. 3: Box plot of the minimum number of RISs obtained by the proposed algorithm and the baselines over thirty runs.

EARA algorithm to others. Through all conceivable configurations of the rate cutoff  $\delta$ , the simulation demonstrates that

the EARA optimizer algorithm has the fewest number of RISs. The EARA optimizer attains a minimal number of RIS that

is equal to N=2, N=3, and N=4 for  $\delta=\{1,1.1,1.2\}$ ,  $\delta=\{1.3,1.4,1.5,1.6\}$ , and  $\delta=\{1.7,1.8,1.9,2\}$ , correspondingly. Furthermore, the AEO and ARO are the EARA-closest algorithms at  $\delta=\{1.1,1.3\}$ . EARA further demonstrated the algorithm's resilience by guaranteeing the nearest values for every run (small box size).

Following the display of the box plot, which illustrates the lowest, median, and maximum number of RISs for each optimization procedure, we simulate in Figure 4 the number of RISs for various optimization strategies. This figure indicates that EARA is superior at all rate threshold values  $\delta$ . When EARA is compared to standard ARO, GO, AEO, and PSO, the average number of RIS is improved by 5.32%, 6.7%, 16.73%, and 20.06%, respectively.

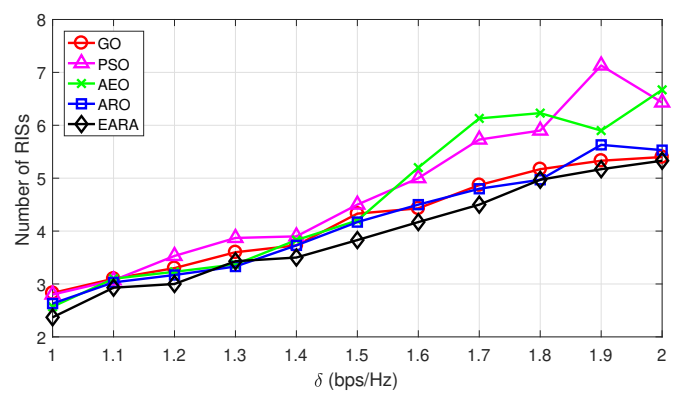


Fig. 4: Number of RISs obtained by the proposed algorithm and the baselines over thirty runs.

A useful metric for contrasting optimization techniques is the fitness value. The fitness value for several algorithms is plotted against the number of iterations in Figure 5. We observed that the value of the rate threshold  $\delta$  is correlated with the number of iterations required for each optimization technique to converge. The number of iterations required grows with the rate  $\delta$ . As stated otherwise, all algorithms converge after 9, 18, 35, 55, 90, and 100 iterations, respectively, for  $\delta=1$ ,  $\delta=1.2$ ,  $\delta=1.4$ ,  $\delta=1.6$ ,  $\delta=1.8$ , and  $\delta=2$ . In addition, the GO, ARO, and EARA algorithms converge more quickly than other algorithms.

Several recent artificial intelligence optimization algorithms are employed in this study to optimize and solve the proposed complex problem. In the context of optimization algorithms, Artificial intelligence (AI) techniques are applied to create algorithms that can adapt, learn, and improve their performance over time. Examples of the AI optimization algorithms employed in our study include standard ARO, GO, AEO, and PSO. We investigated and conducted a more comparative analysis, which is divided into different main parts, as follows:

- 1) Analysis of the performance indices in terms of the obtained Mean, Median, and Success Rate for GO, PSO, AEO, ARO and improved ARO (EARA) for different values of  $\delta$ . (c.f. Table I)
- 2) Analysis of Best and Worst Case Scenarios. This can provide a more comprehensive understanding of its performance across various scenarios. (c.f. Table II)

3) Standard Deviations: Discuss the implications of standard deviations in the obtained results. The proposed EARA provides relatively low standard deviations, which indicate the stability and consistency of the EARA's performance. (c.f. Table II)

Table I displays the mean, median, and success rate <sup>2</sup> for every optimization procedure for various rate values  $\delta$ . While Table II displays the best, worst, and standard deviation for various rate values  $\delta$  for different optimization algorithms. It is observed that for all rate values  $\delta$ , the EARA yields the lowest mean and median of the number of RISs. Furthermore, while considering the success rate in comparison to the other algorithms, the EARA's advantage is rather evident. The EARA is able to reach, at all values of rate threshold  $\delta$ , the minimum number of RISS (Equation (9)). At  $\delta = 1.1, 1.2$ , ARO was unable to reach the minimum, whereas AEO had two failure rates at  $\delta = \{1.6, 1.7\}$ . At  $\delta = 1.2$ , both GO and PSO have a zero success rate. Numerically, at  $\delta = 1.4$ , the EARA promotes improvements in the success rate by 6.66%, 6.66%, 45.43%, and 99% in comparison to AEO, GO, ARO, and PSO.

### V. Conclusion

In this paper, the optimization of wireless communications locations with multi-RIS support is examined. To cut down on the number of RISs exposed to success rates, a novel Enhanced Artificial Rabbits Algorithm Optimizer was suggested to optimize the RISs' positions, numbers, and phase shift coefficients simultaneously. The proposed algorithm's usefulness was illustrated through comparisons with a variety of algorithms, including ARO, GO, AEO, and PSO. The simulation results demonstrate the high efficiency of the proposed EARA algorithm in achieving the highest success rate of obtaining the minimum number of RISs under different threshold values of the achievable rates. The average number of RIS is improved by 5.32%, 6.7%, 16.73%, and 20.06%, respectively, when comparing EARA to standard ARO, GO, AEO, and PSO. Moreover, simulation results show that the EARA increases the success rate at  $\delta = 1.4$  by 6.66%, 6.66%, 45.43%, and 99% in comparison to AEO, GO, ARO, and PSO, respectively.

## REFERENCES

- C.-X. Wang et al., "On the road to 6G: Visions, requirements, key technologies, and testbeds," *IEEE Communications Surveys & Tutorials*, vol. 25, no. 2, pp. 905–974, 2023, doi: 10.1109/COMST.2023.3249835.
- [2] A. Papazafeiropoulos, C. Pan, P. Kourtessis, S. Chatzinotas, and J. M. Senior, "Intelligent reflecting surface-assisted MU-MISO systems with imperfect hardware: Channel estimation and beamforming design," *IEEE Transactions on Wireless Communications*, vol. 21, no. 3, pp. 2077–2092, 2022, doi: 10.1109/TWC.2021.3109391.
- [3] Q. Zhu, Y. Gao, Y. Xiao, M. Xiao, and S. Mumtaz, "Intelligent reflecting surface aided wireless networks: Dynamic user access and system sumrate maximization," *IEEE Transactions on Communications*, vol. 70, no. 4, pp. 2870–2881, 2022, doi: 10.1109/TCOMM.2022.3155147.

<sup>2</sup>The success rate is the number of times, over thirty runs, that the optimization method approaches the least value.

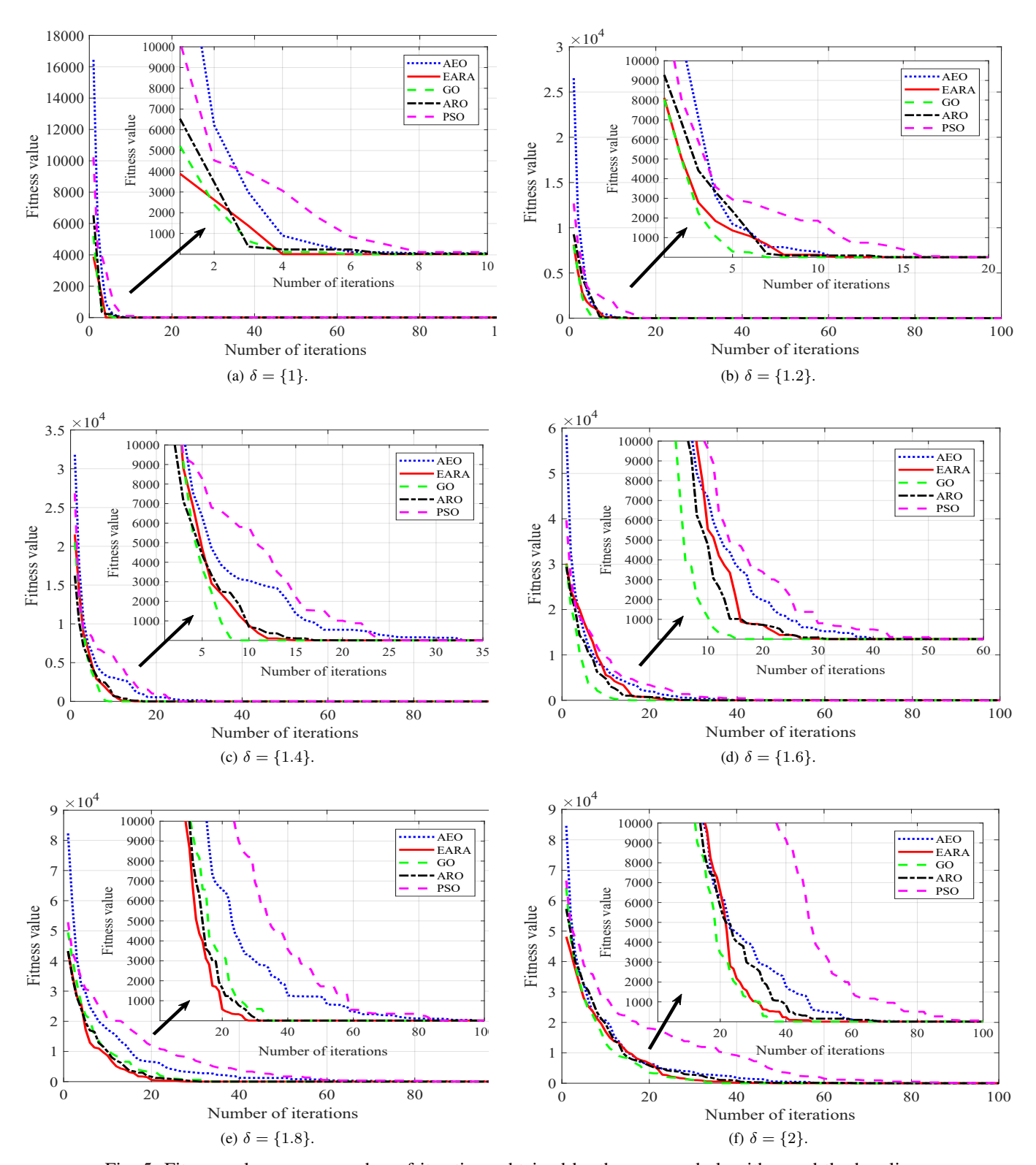


Fig. 5: Fitness value versus number of iterations obtained by the proposed algorithm and the baselines.

- [4] N. T. Nguyen, V.-D. Nguyen, H. V. Nguyen, H. Q. Ngo, S. Chatzinotas, and M. Juntti, "Spectral efficiency analysis of hybrid relay-reflecting intelligent surface-assisted cell-free massive MIMO systems," *IEEE Transactions on Wireless Communications*, vol. 22, no. 5, pp. 3397–3416, 2023, doi: 10.1109/TWC.2022.3217828.
- [5] S. Xu, J. Liu, T. K. Rodrigues, and N. Kato, "Robust multiuser beamforming for irs-enhanced near-space downlink communications
- coexisting with satellite system," *IEEE Internet of Things Journal*, vol. 9, no. 16, pp. 14 900–14 912, 2022, doi: 10.1109/JIOT.2021.3112595.
- [6] V. Kumar, M. F. Flanagan, R. Zhang, and L.-N. Tran, "Achievable rate maximization for underlay spectrum sharing MIMO system with intelligent reflecting surface," *IEEE Wireless Communications Letters*, vol. 11, no. 8, pp. 1758–1762, 2022, doi: 10.1109/LWC.2022.3180988.
- [7] Y. Liu, X. Liu, X. Mu, T. Hou, J. Xu, M. Di Renzo, and N. Al-Dhahir,

TABLE I: Obtained Mean, Median, and Success Rate for GO, PSO, AEO, ARO and improved ARO (EARA) for different value of  $\delta = \{1, 1.1, 1.2, 1.3, 1.4, 1.5, 1.6, 1.7, 1.8, .1.9, 2\}$ .

	Optimization Algorithms									
		GO			PSC	)	AEO			
Phi	Mean	Median	Success Rate	Mean	Median	Success Rate	Mean	Median	Success Rate	
1.00	2.83	3.00	26.67	2.80	3.00	33.33	2.57	3.00	43.33	
1.10	3.10	3.00	10.00	3.07	3.00	16.67	3.10	3.00	3.33	
1.20	3.30	3.00	0.00	3.53	3.00	0.00	3.23	3.00	3.33	
1.30	3.60	3.50	50.00	3.87	4.00	30.00	3.37	3.00	63.33	
1.40	3.73	3.50	50.00	3.90	4.00	26.67	3.83	4.00	40.00	
1.50	4.33	4.00	13.33	4.50	4.50	10.00	4.20	4.00	23.33	
1.60	4.43	4.50	13.33	5.00	5.00	6.67	5.20	5.00	0.00	
1.70	4.87	5.00	3.33	5.73	6.00	0.00	6.13	6.00	0.00	
1.80	5.17	5.00	23.33	5.90	6.00	6.67	6.23	6.00	3.33	
1.90	5.33	5.00	6.67	7.13	6.50	3.33	5.90	6.00	3.33	
2.00	5.40	5.00	6.67	6.43	6.00	3.33	6.67	7.00	6.67	

Optimization Algorithms										
		ARC	)	EARA						
Phi	Mean	Median	Success Rate	Mean	Median	Success Rate				
1.00	2.63	3.00	36.67	2.37	2.00	63.33				
1.10	3.03	3.00	0.00	2.93	3.00	10.00				
1.20	3.17	3.00	0.00	3.00	3.00	13.33				
1.30	3.33	3.00	66.67	3.43	3.00	56.67				
1.40	3.73	4.00	36.67	3.50	3.00	53.33				
1.50	4.17	4.00	13.33	3.83	4.00	26.67				
1.60	4.50	4.00	6.67	4.17	4.00	3.33				
1.70	4.80	5.00	6.67	4.50	4.00	6.67				
1.80	4.97	5.00	36.67	4.97	5.00	33.33				
1.90	5.63	5.00	6.67	5.17	5.00	26.67				
2.00	5.53	5.00	3.33	5.33	5.00	13.33				

TABLE II: Obtained Bes, Worst and Standard Deviation for GO, PSO, AEO, ARO and improved ARO (EARA) for different value of  $\delta = \{1, 1.1, 1.2, 1.3, 1.4, 1.5, 1.6, 1.7, 1.8, 1.9, 2\}$ .

Optimization Algorithms									
	AEO					EARA	GO		
Phi	Best	Worst	Standard Deviation	Best	Worst	Standard Deviation	Best	Worst	Standard Deviation
1	2	3	0.504007	2	3	0.490133	2	4	0.5920935
1.1	2	4	0.402578	2	4	0.365148	2	4	0.5477226
1.2	2	4	0.504007	2	4	0.525226	3	4	0.4660916
1.3	3	4	0.490133	3	4	0.504007	3	5	0.6746647
1.4	3	6	0.833908	3	5	0.572351	3	6	0.9071871
1.5	3	6	0.846901	3	5	0.592093	3	6	0.758098
1.6	4	8	1.063501	3	5	0.461133	3	6	0.8172002
1.7	4	10	1.382984	3	7	0.900192	3	6	0.7760792
1.8	4	9	1.194335	4	7	0.889918	4	7	0.8339078
1.9	4	10	1.09387	4	8	0.949894	4	6	0.6064784
2	4	9	1.49328	4	7	0.802296	4	7	0.6746647

Optimization Algorithms									
			ARO	PSO					
Phi	Best	Worst	Standard Deviation	Best	Worst	Standard Deviation			
1	2	3	0.4901	2	4	0.66436			
1.1	3	4	0.1826	2	5	0.69149			
1.2	3	5	0.4611	3	6	0.68145			
1.3	3	4	0.4795	3	5	0.68145			
1.4	3	5	0.6397	3	5	0.66176			
1.5	3	6	0.7466	3	6	0.82001			
1.6	3	7	0.861	3	8	1.23176			
1.7	3	6	0.7611	4	9	1.14269			
1.8	4	8	1.0334	4	8	0.95953			
1.9	4	9	1.0334	4	10	1.77596			
2	4	8	0.9371	4	10	1.47819			

<sup>&</sup>quot;Reconfigurable intelligent surfaces: Principles and opportunities," *IEEE Communications Surveys & Tutorials*, vol. 23, no. 3, pp. 1546–1577, 2021, doi: 10.1109/COMST.2021.3077737.

<sup>[8]</sup> B. Mao, Y. Kawamoto, and N. Kato, "AI-based joint optimization of QoS and security for 6G energy harvesting internet of things," *IEEE Internet of Things Journal*, vol. 7, no. 8, pp. 7032–7042, 2020, doi: 10.1109/JIOT.2020.2982417.

<sup>[9]</sup> Z. Wang, L. Liu, S. Zhang, and S. Cui, "Massive MIMO com-

munication with intelligent reflecting surface," *IEEE Transactions on Wireless Communications*, vol. 22, no. 4, pp. 2566–2582, 2023, doi: 10.1109/TWC.2022.3212537.

<sup>[10]</sup> M. I. Ismail, A. M. Shaheen, M. M. Fouda, and A. S. Alwakeel, "RIS-assisted integrated sensing and communication systems: Joint reflection and beamforming design," *IEEE Open Journal of the Communications Society*, early access, 2024, doi: 10.1109/OJCOMS.2024.3353770.

<sup>[11]</sup> M. Matthaiou, O. Yurduseven, H. Q. Ngo, D. Morales-Jimenez, S. L.

- Cotton, and V. F. Fusco, "The road to 6G: Ten physical layer challenges for communications engineers," *IEEE Communications Magazine*, vol. 59, no. 1, pp. 64–69, 2021, doi: 10.1109/MCOM.001.2000208.
- [12] W. Saad, M. Bennis, and M. Chen, "A vision of 6G wireless systems: Applications, trends, technologies, and open research problems," *IEEE Network*, vol. 34, no. 3, pp. 134–142, 2020, doi: 10.1109/MNET.001.1900287.
- [13] A. Taha, M. Alrabeiah, and A. Alkhateeb, "Deep learning for large intelligent surfaces in millimeter wave and massive MIMO systems," in 2019 IEEE Global Communications Conference (GLOBECOM), 2019, doi: 10.1109/GLOBECOM38437.2019.9013256.
- [14] B. Ling, J. Lyu, and L. Fu, "Placement optimization and power control in intelligent reflecting surface aided multiuser system," in 2021 IEEE Global Communications Conference (GLOBECOM), 2021, doi: 10.1109/GLOBECOM46510.2021.9686030.
- [15] G. Ghatak, "On the placement of intelligent surfaces for RSSI-based ranging in Mm-Wave networks," *IEEE Communications Letters*, vol. 25, no. 6, pp. 2043–2047, 2021, doi: 10.1109/LCOMM.2021.3063918.
- [16] S. Huang, B. Wang, Y. Zhao, and M. Luan, "Near-field RSS-based localization algorithms using reconfigurable intelligent surface," *IEEE Sensors Journal*, vol. 22, no. 4, pp. 3493–3505, 2022, doi: 10.1109/JSEN.2022.3141386.
- [17] Y. Fang, S. Atapattu, H. Inaltekin, and J. Evans, "Optimum reconfigurable intelligent surface selection for wireless networks," arXiv: 2012.11793, 2020, doi: 10.48550/arXiv.2012.11793.
- [18] W. Mei and R. Zhang, "Cooperative beam routing for multi-IRS aided communication," *IEEE Wireless Communications Letters*, vol. 10, no. 2, pp. 426–430, 2021, doi: 10.1109/LWC.2020.3034370.
- [19] Z. Yang, M. Chen, W. Saad, W. Xu, M. Shikh-Bahaei, H. V. Poor, and S. Cui, "Energy-efficient wireless communications with distributed reconfigurable intelligent surfaces," *IEEE Transactions on Wireless Communications*, vol. 21, no. 1, pp. 665–679, 2022, doi: 10.1109/TWC.2021.3098632.
- [20] J. Lyu and R. Zhang, "Spatial throughput characterization for intelligent reflecting surface aided multiuser system," *IEEE Wireless Communications Letters*, vol. 9, no. 6, pp. 834–838, 2020, doi: 10.1109/LWC.2020.2972527.
- [21] G. C. Alexandropoulos, S. Samarakoon, M. Bennis, and M. Debbah, "Phase configuration learning in wireless networks with multiple reconfigurable intelligent surfaces," in 2020 IEEE Globecom Workshops (GC Wkshps, 2020, doi: 10.1109/GCWkshps50303.2020.9367575.
- [22] I. Yildirim, A. Uyrus, and E. Basar, "Modeling and analysis of reconfigurable intelligent surfaces for indoor and outdoor applications in future wireless networks," *IEEE Transactions on Communications*, vol. 69, no. 2, pp. 1290–1301, 2021, doi: 10.1109/TCOMM.2020.3035391.
- [23] S. Zhang and R. Zhang, "Capacity characterization for intelligent reflecting surface aided MIMO communication," *IEEE Journal on Selected Areas in Communications*, vol. 38, no. 8, pp. 1823–1838, 2020, doi: 10.1109/JSAC.2020.3000814.
- [24] X. Xie, H. Tang, H. Yang, Q. Huang, and D. Pu, "Intelligent reflecting surface assisted wireless information and power transfer with X-duplex for 6G networks," *IEEE Systems Journal*, vol. 16, no. 4, pp. 5894–5905, 2022, doi: 10.1109/JSYST.2021.3120299.
- [25] B. Zheng and R. Zhang, "Intelligent reflecting surface-enhanced ofdm: Channel estimation and reflection optimization," *IEEE Wireless Communications Letters*, vol. 9, no. 4, pp. 518–522, 2020, doi: 10.1109/LWC.2019.2961357.
- [26] G. Zhou, C. Pan, H. Ren, K. Wang, M. D. Renzo, and A. Nallanathan, "Robust beamforming design for intelligent reflecting surface aided MISO communication systems," *IEEE Wireless Communications Letters*, vol. 9, no. 10, pp. 1658–1662, 2020, doi: 10.1109/LWC.2020.3000490.
- [27] W. Shi, J. Li, G. Xia, Y. Wang, X. Zhou, Y. Zhang, and F. Shu, "Secure multigroup multicast communication systems via intelligent reflecting surface," *China Communications*, vol. 18, no. 3, pp. 39–51, 2021, doi: 10.23919/JCC.2021.03.004.
- [28] S. Abeywickrama, R. Zhang, Q. Wu, and C. Yuen, "Intelligent reflecting surface: Practical phase shift model and beamforming optimization," *IEEE Transactions on Communications*, vol. 68, no. 9, pp. 5849–5863, 2020, doi: 10.1109/TCOMM.2020.3001125.
- [29] J. An, L. Wang, C. Xu, L. Gan, and L. Hanzo, "Optimal pilot power based channel estimation improves the throughput of intelligent reflective surface assisted systems," *IEEE Transactions on Vehicular Technology*, vol. 69, no. 12, pp. 16202–16206, 2020, doi: 10.1109/TVT.2020.3034478.
- [30] R. Hashemi, S. Ali, N. H. Mahmood, and M. Latva-Aho, "Joint sum rate and blocklength optimization in RIS-aided short packet URLLC

- systems," *IEEE Communications Letters*, vol. 26, no. 8, pp. 1838–1842, 2022, doi: 10.1109/LCOMM.2022.3180396.
- [31] H. Xie, J. Xu, Y.-F. Liu, L. Liu, and D. W. K. Ng, "User grouping and reflective beamforming for IRS-aided URLLC," *IEEE Wireless Communications Letters*, vol. 10, no. 11, pp. 2533–2537, 2021, doi: 10.1109/LWC.2021.3106548.
- [32] Y. Zhu, Z. Bo, M. Li, Y. Liu, Q. Liu, Z. Chang, and Y. Hu, "Deep reinforcement learning based joint active and passive beamforming design for RIS-assisted MISO systems," in 2022 IEEE Wireless Communications and Networking Conference (WCNC), 2022, doi: 10.1109/WCNC51071.2022.9771666. pp. 477–482.
- [33] C. Huang, G. Chen, Y. Gong, M. Wen, and J. A. Chambers, "Deep reinforcement learning-based relay selection in intelligent reflecting surface assisted cooperative networks," *IEEE Wireless Communications Letters*, vol. 10, no. 5, pp. 1036–1040, 2021, doi: 10.1109/LWC.2021.3056620.
- [34] Y. Yang, B. Zheng, S. Zhang, and R. Zhang, "Intelligent reflecting surface meets OFDM: Protocol design and rate maximization," *IEEE Transactions on Communications*, vol. 68, no. 7, pp. 4522–4535, 2020, doi: 10.1109/TCOMM.2020.2981458.
- [35] Y. Li, M. Jiang, Q. Zhang, and J. Qin, "Joint beamforming design in multi-cluster MISO NOMA reconfigurable intelligent surface-aided downlink communication networks," *IEEE Transac*tions on Communications, vol. 69, no. 1, pp. 664–674, 2021, doi: 10.1109/TCOMM.2020.3032695.
- [36] S. H. Zainud-Deen, "Reconfigurable intelligent surfaces for wireless communications," in 2022 39th National Radio Science Conference (NRSC), vol. 1, 2022, doi: 10.1109/NRSC57219.2022.9971201.
- [37] C. Huang, Z. Yang, G. C. Alexandropoulos, K. Xiong, L. Wei, C. Yuen, Z. Zhang, and M. Debbah, "Multi-hop RIS-empowered terahertz communications: A DRL-based hybrid beamforming design," *IEEE Journal* on Selected Areas in Communications, vol. 39, no. 6, pp. 1663–1677, 2021, doi: 10.1109/JSAC.2021.3071836.
- [38] I. Trigui, W. Ajib, W.-P. Zhu, and M. D. Renzo, "Performance evaluation and diversity analysis of RIS-assisted communications over generalized fading channels in the presence of phase noise," *IEEE Open Jour*nal of the Communications Society, vol. 3, pp. 593–607, 2022, doi: 10.1109/OJCOMS.2022.3160722.
- [39] Y. Gao, J. Xu, W. Xu, D. W. K. Ng, and M.-S. Alouini, "Distributed IRS with statistical passive beamforming for MISO communications," *IEEE Wireless Communications Letters*, vol. 10, no. 2, pp. 221–225, 2021, doi: 10.1109/LWC.2020.3024952.
- [40] Z. Kang, C. You, and R. Zhang, "IRS-aided wireless relaying: Deployment strategy and capacity scaling," *IEEE Wireless Communications Letters*, vol. 11, no. 2, pp. 215–219, 2022, doi: 10.1109/LWC.2021.3123075.
- [41] S. Zhang and R. Zhang, "Intelligent reflecting surface aided multiuser communication: Capacity region and deployment strategy," *IEEE Transactions on Communications*, vol. 69, no. 9, pp. 5790–5806, 2021, doi: 10.1109/TCOMM.2021.3079128.
- [42] Q. Wu, S. Zhang, B. Zheng, C. You, and R. Zhang, "Intelligent reflecting surface-aided wireless communications: A tutorial," *IEEE Transactions on Communications*, vol. 69, no. 5, pp. 3313–3351, 2021, doi: 10.1109/TCOMM.2021.3051897.
- [43] N. U. Saqib, S. Hou, S. H. Chae, and S.-W. Jeon, "Ris-aided wireless indoor communication: Sum rate maximization via RIS placement optimization," in *ICC* 2023 - *IEEE International Conference on Commu*nications, 2023, doi: 10.1109/ICC45041.2023.10278693. pp. 511–516.
- [44] R. S. P. Sankar and S. P. Chepuri, "Channel-aware placement of active and passive elements in hybrid RIS-assisted MISO systems," *IEEE Wireless Communications Letters*, vol. 12, no. 7, pp. 1229–1233, 2023, doi: 10.1109/LWC.2023.3268359.
- [45] Y. Pan, Z. Qin, J.-B. Wang, Y. Chen, H. Yu, and A. Tang, "Joint deployment and beamforming design for STAR-RIS aided communication," *IEEE Communications Letters*, vol. 27, no. 11, pp. 3083–3087, 2023, doi: 10.1109/LCOMM.2023.3316620.
- [46] M. P. Reddy, S. Amuru, and K. K. Kuchi, "Optimizing the placement and beamforming of RIS in cellular networks: A system-level modeling perspective," *IEEE Communications Letters*, vol. 27, no. 12, pp. 3399– 3403, 2023, doi: 10.1109/LCOMM.2023.3329135.
- [47] C. Liu, R. He, Y. Niu, Z. Han, B. Ai, M. Gao, Z. Ma, G. Wang, and Z. Zhong, "Reconfigurable intelligent surface assisted high-speed train communications: Coverage performance analysis and placement optimization," *IEEE Transactions on Vehicular Technology*, pp. 1–16, 2023, doi: 10.1109/TVT.2023.3325627.
- [48] L. Wang, Q. Cao, Z. Zhang, S. Mirjalili, and W. Zhao, "Artificial rabbits optimization: A new bio-inspired meta-heuristic algorithm for solving engineering optimization problems," *Engineering Applications*

- of Artificial Intelligence, vol. 114, article no. 105082, 2022, doi: 10.1016/j.engappai.2022.105082.
- [49] M. Elshahed, M. A. Tolba, A. M. El-Rifaie, A. Ginidi, A. Shaheen, and S. A. Mohamed, "An artificial rabbits' optimization to allocate pvstatcom for ancillary service provision in distribution systems," Mathematics, vol. 11, no. 2, p. 339, 2023, doi: 10.3390/math11020339.
- [50] R. El-Sehiemy, A. Shaheen, A. Ginidi, and S. F. "Proportional-integral-derivative controller based-artificial rabbits algorithm for load frequency control in multi-area power systems," Fractal and Fractional, vol. 7, no. 1, p. 97, 2023, doi: 10.3390/fractalfract7010097
- [51] A. Mahdy, A. Shaheen, R. El-Sehiemy, and A. Ginidi, "Artificial ecosystem optimization by means of fitness distance balance model for engineering design optimization," The Journal of Supercomputing, vol. 79, pp. 1-32, 2023, doi: 10.1007/s11227-023-05331-y.
- [52] H. B. Aribia, A. M. El-Rifaie, M. A. Tolba, A. Shaheen, G. Moustafa, F. Elsayed, and M. Elshahed, "Growth optimizer for parameter identification of solar photovoltaic cells and modules," Sustainability, vol. 15, no. 10, 2023, doi: 10.3390/su15107896.
- [53] M. Almseidin, J. Al-Sawwa, M. Alkasassbeh, M. Alzubi, and K. Alrfou, "DT-ARO: Decision tree-based artificial rabbits optimization to mitigate iot botnet exploitation," Journal of Network and Systems Management, vol. 32, no. 1, p. 14, 2024.
- [54] H. Bakır, "Dynamic fitness-distance balance-based artificial rabbits optimization algorithm to solve optimal power flow problem," Expert Systems with Applications, vol. 240, p. 122460, 2024, doi: https://doi.org/10.1016/j.eswa.2023.122460.
- [55] M. Kharrich, M. H. Hassan, S. Kamel, and J. Kim, "Designing an optimal hybrid microgrid system using a leader artificial rabbits optimization algorithm for domestic load in Guelmim city, Morocco," Renewable Energy, vol. 223, p. 120011, 2024, doi: https://doi.org/10.1016/j.renene.2024.120011.
- [56] M. Li, Z. Cui, and T. Fan, "The flood simulation of the modified muskingum model with a variable exponent based on the artificial rabbit optimization algorithm," Water, vol. 16, no. 2, 2024, doi: 10.3390/w16020339.
- [57] B. Ozkaya, S. Duman, H. T. Kahraman, and U. Guvenc, "Optimal solution of the combined heat and power economic dispatch problem by adaptive fitness-distance balance based artificial rabbits optimization algorithm," Expert Systems with Applications, vol. 238, p. 122272, 2024, doi: https://doi.org/10.1016/j.eswa.2023.122272.
- [58] A. E. Khalil, T. A. Boghdady, M. H. Alham, and D. K. Ibrahim, "Enhancing the conventional controllers for load frequency control of isolated microgrids using proposed multi-objective formulation via artificial rabbits optimization algorithm," IEEE Access, vol. 11, pp. 3472-3493, 2023, doi: 10.1109/ACCESS.2023.3234043.
- [59] L. A. Alharbi, "Artificial rabbits optimizer with machine learning based emergency department monitoring and medical data classification at KSA hospitals," IEEE Access, vol. 11, pp. 59133-59141, 2023, doi: 10.1109/ACCESS.2023.3284390
- [60] A. Mazloumi, A. Poolad, M. S. Mokhtari, M. B. Altman, A. Y. Abdelaziz, and M. Elsisi, "Optimal sizing of a photovoltaic pumping system integrated with water storage tank considering cost/reliability assessment using enhanced artificial rabbits optimization: A case study, Mathematics, vol. 11, no. 2, 2023, doi: 10.3390/math11020463.

## VI. APPENDIX

## Algorithm 1 Proposed EARA

33:

34:

35:

score  $(AR_S)$ 

36: end procedure

end while

**Input:** Population size  $(N_{AR})$ , Maximum iterations number  $(t_{max})$ , upper lower bounds (Up and Lo)

```
Output: Best RIS elements and their installed positions
 1: procedure EARA
 2: Set t = 1
 3: Initialize AR_k, using Eq. (10)
 4: Assign to the design variables
 5: Round the number of RIS to be placed and extract their
    distribution patterns
       for k = 1 : N_{AR} do
 6:
           Evaluate \Delta GK using Eq. (24)
 7:
 8:
           Evaluate \Delta GH using Eq. (23)
 9:
           Evaluate the fitness of the rabbit location f(AR_k)
    using Eq.(22)
       end for
10:
       Extract the best position with the minimum fitness
11:
    score (AR_S)
       while t < t_{max} do
12:
           for k = 1 : N_{AR} do
13:
               Evaluate EF(t) using Equ. (18)
14:
               if EF(t) < 1 then
15:
                   Update AR_k^* using Equ. (16)
16:
               else
17:
                   Update AR_k^* using Equ. (16)
18:
                   Generate a random number (RN) inside the
19:
    range [0,1]
                   if RN > TF(t) then
20:
                       Update AR_k^* via Equ. (11)
21:
22:
                       update AR_k^* via Equ. (19)
23:
                   end if
24:
               end if
25:
               Assign to the design variables
26:
27:
               Round the number of RIS to be placed and
    extract their distribution patterns
               Evaluate \Delta GK using Equ. (24)
28:
29:
               Evaluate \Delta GH using Equ. (23)
               Evaluate the fitness of the rabbit location
30:
    (f(AR_k^*)) using Equ. (22)
               Update the rabbit location using Equ (17)
31:
32:
           Update the best position with the minimum fitness
```

Print the best RIS elements and their installed posi-

tions regarding the best position  $(AR_S)$ 



Ahmed S. Alwakeel received the B.S. degree in electronics and communications engineering from Cairo University, Giza, Egypt, in 2006, and the M.S. degree in electronics and communications from Port Said University, Port Fuad, Egypt, in 2014, and the Ph.D. degree in communications and electronics department, Suez Canal University, Ismailia, Egypt, in 2018. He is currently an Assistant Professor in Suez University. His current research interests include large-scale (massive) MIMO systems, cooperative communications, and interference networks.



grids.

Abdullah M. Shaheen was born in Tanta, Egypt, in 1985. He received the B.Sc. degree from Suez Canal University, Port-Said, Egypt, in 2007, and the M.Sc. and Ph.D. degrees from Menoufia University, Shebin El-Kom, Egypt, in 2012 and 2016, respectively. He is currently with the Department of Electrical Engineering, Faculty of Engineering, Suez University, El-Suweis, Egypt. His research interests include power system operation, control, and planning, the applications of optimization algorithms in electric power systems, renewable integration, and smart



Mohamed I. Ismail is an Assistant Professor at Modern Academy for Engineering and Technology, with expertise in signal processing, communication networks, MIMO systems, cooperative communications, and interference networks. He earned his B.S. degree in electronics and communications engineering from Modern Academy for Engineering and Technology, Cairo, Egypt in 2008, followed by an M.S. degree in electronics and communications from AASTMT- Arab Academy for Science, Technology and Maritime Transport Cairo, Egypt in 2014. In

2019, he received his Ph.D. degree in communications and electronics department from Suez Canal University, Ismailia, Egypt. Dr. Ismail has made significant contributions to the field of engineering and international relations. He was a member of the Committee of International Relations and African Affairs at the Egyptian Engineering Syndicate "ESE" from 2017 to 2022, where he contributed to the capacity-building program for international fresh graduate engineers. He was also a member of the strategic planning committee at the Federation of African Engineering Organization "FAEO" from 2020 to 2022. Additionally, he represented the ESE in Zambia to activate the protocol of the capacity-building program between the ESE and the Engineering institution of Zambia EIZ from 2019 to 2020.



Adel Khaled received the B.S. degree in electronics and communications engineering from Port Said University, Port Fuad, Egypt, in 2007, and the M.S. degree in electronics and communications from Port Said University, Port Fuad, Egypt, in 2014, and the Ph.D. degree in communications and electronics department, Port Said University, Port Fuad, Egypt, in 2021. The current Position is an Assistant Professor in Faculty of Engineering Suez University, Egypt. The research interests include large-scale (massive) MIMO systems, Wireless Communications, Signal

Processing, Mobile Communications.



Mostafa M. Fouda (Senior Member, IEEE) received the B.S. degree and the M.S. degree in Electrical Engineering from Benha University, Egypt, in 2002 and 2007, respectively, and the Ph.D. degree in Information Sciences from Tohoku University, Japan, in 2011. He is an Associate Professor with the Department of Electrical and Computer Engineering at Idaho State University, ID, USA. He also holds the position of a Full Professor at Benha University. He was an Assistant Professor at Tohoku University and a Postdoctoral Research Associate at Tennessee

Technological University, TN, USA. He has (co)authored more than 230 technical publications. His current research focuses on cybersecurity, communication networks, signal processing, wireless mobile communications, smart healthcare, smart grids, AI, and IoT. He has guest-edited several special issues covering various emerging topics in communications, networking, and health analytics. He currently serves on the editorial board of IEEE Transactions on Vehicular Technology (TVT), IEEE Internet of Things Journal (IoT-J), and IEEE Access. He has received several research grants, including NSF Japan-U.S. Network Opportunity 3 (JUNO3). He is a Senior Member of IEEE.